Cancer Immunology, Immunotherapy (2025) 74:80
https://doi.org/10.1007/s00262-024-03935-8

RESEARCH

Pre-immunotherapy alters stereotactic ablative radiotherapy-induced systemic T cell responses in early-stage NSCLC

Chao Liu[1] · Yanjuan Chen[2] · Xiaohui Li[3] · Zhijie Bai[4] · Meilin Jiang[5] · Dongsheng Sheng[6] · Wenxue Zou[7] · Rui Huang[7] · Qingyu Huang[7] · Fuhao Wang[7] · Jingyang Zhu[8] · Huiru Sun[8] · Bing Liu[4] · Zongcheng Li[4] · Bing Sun[8]

Received: 8 July 2024 / Accepted: 27 December 2024 / Published online: 1 February 2025

Abstract

Background Stereotactic ablative radiotherapy (SABR) is thought to activate T cell responses in patients with cancer, leading to its combination with immunotherapy and chemotherapy for treatment of non-small-cell lung cancer (NSCLC). Here, we aimed to provide a high-resolution transcriptomic profiling of the systemic T cell response following SABR, with or without preceding immunotherapy/chemotherapy.

Methods We conducted single-cell RNA and T cell receptor (TCR) sequencing of T cells from peripheral blood of seven patients with early-stage NSCLC taken pre- and post-SABR without or with prior immunotherapy and chemotherapy (icSABR). Other flow cytometry, single-cell RNA-seq data and bulk RNA-seq data were used to validate the results.

Results We uncovered distinct T cell response patterns induced by these treatments: while terminal effector $CD8^+$ T cells showed increased cytotoxic and inhibitory scores, and upregulated immune-activated pathways post-SABR, the reverse responses occurred post-icSABR. Furthermore, the proportion of large T cell clones increased and single clone decreased post-SABR, while the opposite was seen post-icSABR. Of note, both SABR and icSABR largely changed TCR clonotypes, which were mainly large clones post-SABR but single clone post-icSABR, and predominantly from terminal effector $CD8^+$ T cells and T helper cells, respectively.

Conclusions These findings reveal a complex interplay between SABR and immunotherapy, with potentially valuable implications for treatment strategies involving SABR and immunotherapy to induce systemic T cell responses for tumor eradication in patients with NSCLC.

Keywords SABR · Non-small-cell lung cancer · Immunotherapy · Single-cell RNA sequencing · Immune response

Introduction

Stereotactic ablative radiotherapy (SABR) uses real-time imaging to guide the application of high doses of radiotherapy into tumors, while sparing surrounding tissues [1]. This approach is now the standard-of-care for patients with inoperable early-stage non-small cell lung cancer (NSCLC), achieving a local control rate of 85–96% in this group [2–5]. Moreover, there is accumulating evidence that SABR modulates immune responses to cancer, acting as a means of "in situ vaccination" that activates immune responses to tumor antigens with the potential to trigger the so-called abscopal effect [6, 7]. Induction of the abscopal effect, where immune-mediated control of distant metastases is initiated by local radiotherapy treatment at a different site, is the ultimate ambition of cancer therapy, and—although rare—has typically occurred 2 months after SABR [8]. It has been suggested that combining SABR and immunotherapy could promote the abscopal effect by enhancing tumor antigen exposure and presentation, increasing T cell killing function, and supporting effector T cell migration into both irradiated and non-irradiated tumor deposits [9], but the immune response to SABR and the immunological interplay between SABR and cancer immunotherapies remain incompletely defined.

Analysis of the cellular components and cytokine profile of peripheral blood has advanced our understanding of how SABR modulates systemic immune activation. In patients with NSCLC, the pro-inflammatory effects of SABR are seen in increased proportions of peripheral $CD4^+$, $CD8^+$

Chao Liu, Yanjuan Chen and Xiaohui Li contributed equally to this work.

Extended author information available on the last page of the article

and NK cells, coupled with decreased proportions of regulatory T cells (Tregs), and the induction of inflammatory cytokines including IL-2, TNF-α and IFN-γ [10–15]. T cell receptor (TCR) sequencing has further revealed increased frequencies of T cell clones recognizing tumor antigens among peripheral T cells after SABR [16, 17]. When combined with immune checkpoint inhibitor (ICI) treatment in patients with melanoma, SABR also increases the frequency of *ICOS*-expressing activated $CD4^+$ T cells and the intensity of *HLA-DR* expression on $CD14^+$ monocytes, while decreasing the frequency of myeloid derived suppressor cells [18, 19]. While these studies have provided important indications of the broad effects of SABR alone or with ICI treatment, the bulk cellular analyses employed are unable to accurately delineate alterations in systemic immune activation due to their inability to account for the critical aspect of cellular heterogeneity within immune populations. The importance of this factor has been revealed with the advent of single-cell RNA sequencing (scRNA-seq) [20]. However, there is a notable absence in high-resolution assessment of the systemic T cell transcriptional and clonal response subsequent to SABR, as well as the influence of pre-treatment immunotherapy and chemotherapy on these responses.

We hypothesized that SABR was inducing profound and lasting changes in T cells, and that the effects of prior immunotherapy and chemotherapy might alter SABR-induced changes in ways that could be impactful for patients' treatment. Here, we combined scRNA-seq and scTCR-seq to characterize the changes in T cell populations, in individual T cell transcriptomes, and in T cell clonality that were induced in patients with early-stage NSCLC by treatment with SABR alone or SABR with prior anti-PD-1 immunotherapy and chemotherapy. We identified two distinct patterns of systemic T cell activation after SABR and icSABR therapy at single-cell resolution, providing unprecedented insight into the immune-modulatory role of SABR, and revealing its complex interactions with immunotherapy and chemotherapy.

Methods

Patients and sample collection

This study was approved by the Ethical Committee of the Fifth Medical Center of Chinese PLA General Hospital (KY-2019-2-6). All patients provided written informed consent prior to sample collection. Seven patients with pathologically confirmed early-stage NSCLC were enrolled in this study, of which four (P001-004) received SABR, and three (P005-P007) received icSABR (SABR preceded by 4 or 6 cycles anti-PD-1 therapy and chemotherapy with nab-paclitaxel combined with cisplatin). A validation cohort included 8 patients with early-stage NSCLC receiving SABR for flow cytometry analysis. The clinical characteristics of enrolled patients are summarized in Supplementary Table 1 and 2. Samples of peripheral blood were collected 1–3 days before radiotherapy and 1–2 months after radiotherapy [11, 12, 17]. Fresh blood was gathered into vacuum tubes separately and then transported in a 4 °C incubator. At the most recent 14-month follow-up period, one patient developed metastases. To support the findings in our data, we included two published datasets of T cells, including one scRNA-seq dataset (GSE202374) and one bulk RNA-seq dataset (GSE153262) from patients with human renal cell carcinoma who underwent SABR [17, 21].

Sample preparation, cell sorting and analysis by flow cytometry

Peripheral blood mononuclear cells (PBMCs) were isolated from fresh blood by density gradient centrifugation over HISTOPAQUE-1077 (Sigma-Aldrich), according to the manufacturer's instructions. Cells from different patients were labeled with unique hashtag antibodies (Biolegend) at 4 °C for 30 min in the dark, before incubation with BV421-conjugated anti-human CD45 (BD, Cat#563,879) and BV605-conjugated anti-human CD3 (BD, Cat# 563,219) at 4 °C for 15 min in the dark. Lastly, the cells were incubated with 7-AAD Viability Staining Solution (eBioscience) at 4 °C for 3 min. Live $CD45^+CD3^+$ T cells were then isolated using a BD FACSAria II. Single-cell libraries were generated from cell suspensions using chromium single-cell 5' library and gel beads kit v2 (10X Genomics Chromium Single Cell platform, Pleasanton, CA, USA) as per the manufacturer's protocol, and their mRNAs were sequenced using the Illumina platform (Illumina, San Diego, CA). In addition, cells were also labeled with PE-Cy7-conjugated anti-human CD8 (BD, Cat# 557,746), APC-conjugated anti-human GZMB (Biolegend, Cat# 372,204), and PE-conjugated anti-human CD223 (LAG3, Biolegend, Cat# 369,205) to identify CD8_TE.

Sequencing and preprocessing

The scRNA-seq datasets at the 5′ end were produced with the 10X Genomics Chromium system (https://support.10xgenomics.com/). FQSTA files with distinct hashtag oligonucleotide (HTO) barcodes were pooled together and processed following the manufacturer's instructions. Raw reads were aligned to the hg19 human reference genome, with gene expression and HTO quantified using *CellRanger* (version 3.0.1), according to the instructions (https://support.10xgenomics.com/single-cell-gene-expression/software). T cell receptor (TCR) profiles were recognized using the 'vdj' subcommands of *CellRanger*.

Quality control

A total of fourteen datasets (pre- and post-therapy from all seven patients) were generated and underwent several layers of quality control. First, samples were split into single batch datasets according to the HTO barcodes. The HTO data were normalized using "NormalizeData" functions with the "CLR" normalization method, and each cell was assigned to its sample-of-origin. Singlets were identified using the "HTODemux" function in *Seurat* package [22–24](version 4.3.0, implemented in *R* software), following the tutorial at https://satijalab.org/, and were retained. Next, those cells expressing more than 600 and fewer than 30,000 genes, with over 1,500 unique molecular identifiers (UMI) and less than 10% of UMIs mapped to mitochondrial genes, were retained for subsequent analysis. Finally, a total of 57,738 cells, comprising 28,382 from the icSABR group, and 29,356 from the SABR group were used. Besides, genes expressed in fewer than 3 cells were excluded from analysis.

Cell clustering and dimensionality reduction

Firstly, to remove batch effects between different samples, pooled UMI data were subjected to canonical correlation analysis (CCA) [22, 24] in Seurat, which is based on identification of 'anchors' between pairs of datasets, by following the tutorial at https://satijalab.org/seurat/v3.1/integration.html. For each sample, the gene expression matrix was normalized using the "NormalizeData" function with default parameters. "FindVariableFeatures" and "SelectIntegrationFeatures" function in Seurat, with nfeatures = 2,500 was used to identify highly variable genes (HVGs). To mitigate the effect of cell cycle, the *Pearson* correlation coefficient of HVGs with each of both cell cycle scores were calculated, and then genes with a correlation coefficient greater than 0.3 were removed from the HVG list. Using the refined HVG list, the "FindIntegrationAnchors" function was applied to compute anchors, with the "IntegrateData" function used to integrate different datasets, employing the parameters dims = 1:15. "ScaleData" and "RunPCA" functions were applied to the integrated expression matrix with default parameters; then, the top 15 most significant principal components were selected and used to perform dimensionality reduction and clustering in Seurat. Cells were projected into a two-dimensional space using uniform manifold approximation and projection (UMAP), and clusters were identified using the "FindClusters" function in Seurat.

We performed the procedure described above three times. In the first round, a single outlying population that did not express *CD3E* was filtered out. In the second round, a population expressing *CD68* while lacking *CD3E*, *CD4* and *CD8A* was further excluded, due to the likelihood of containing monocytes or macrophages. The third and final round of analysis was thus conducted on a high-quality population of T cells, to which the "FindClusters" function in Seurat was applied using a resolution of 2.8. This led to the identification of fourteen T cell clusters.

Identification and analysis of differentially expressed genes (DEGs)

The 'FindMarkers' and 'FindAllMarkers' functions in Seurat were used to identify DEGs between different clusters. The parameters were set only.pos = TRUE, and test.use = "wilcox". Genes with fold change > 1.5 and adjusted *P* value < 0.05 were considered as statistically significant DEGs. The DEGs are listed in the Supplementary Tables 3, 4, 5, and 6.

Cell cycle phase analysis

The "CellCycleScoring" function in Seurat was performed for cell cycle analysis, using a previously reported core gene set consisting of 43 G1/S genes and 54 G2/M genes [25, 26].

Validation of cluster identities in SingleR analysis

The *SingleR* package [27] (version 1.10.0, implemented in *R* software) was used for unsupervised recognition of different cell types. The HumanPrimaryCellAtlasData [28], BlueprintEncodeData [29, 30] and NovershternHematopoieticData [31] were chosen as reference datasets. The top 30 most similar cell types are displayed in the heatmaps.

Feature genes score

Five kinds of feature gene sets were recognized from several previous studies [26, 32–35], including four genes whose expression is associated with naïve T cells (*CCR7, TCF7, LEF1, SELL*), eight genes associated with cytotoxic T cells (*GNLY, NKG7, CST7, PRF1, GZMA, GZMB, GZMH, FGFBP2*), six genes involved in T cell costimulation (*TNFRSF9, TNFRSF14, CD28, ICOS, CD226, TNFRSF25*), five genes with inhibitory functions (*PDCD1, TIGIT, LAG3, HAVCR2, CTLA4*), and five genes associated with Treg cells (*FOXP3, CTLA4, TGFB1, IL10, IL2RA*). Then, the "AddModuleScore" function in Seurat was used to calculate the feature scores. The significance level of the differences in the feature scores between pre- and post-therapy groups was evaluated using the Wilcox test, with *P* values < 0.05 considered as statistically significant.

Gene set enrichment analysis (GSEA)

The enrichment pathways among the DEGs of CD8_TE and proliferating T cluster compared post- with

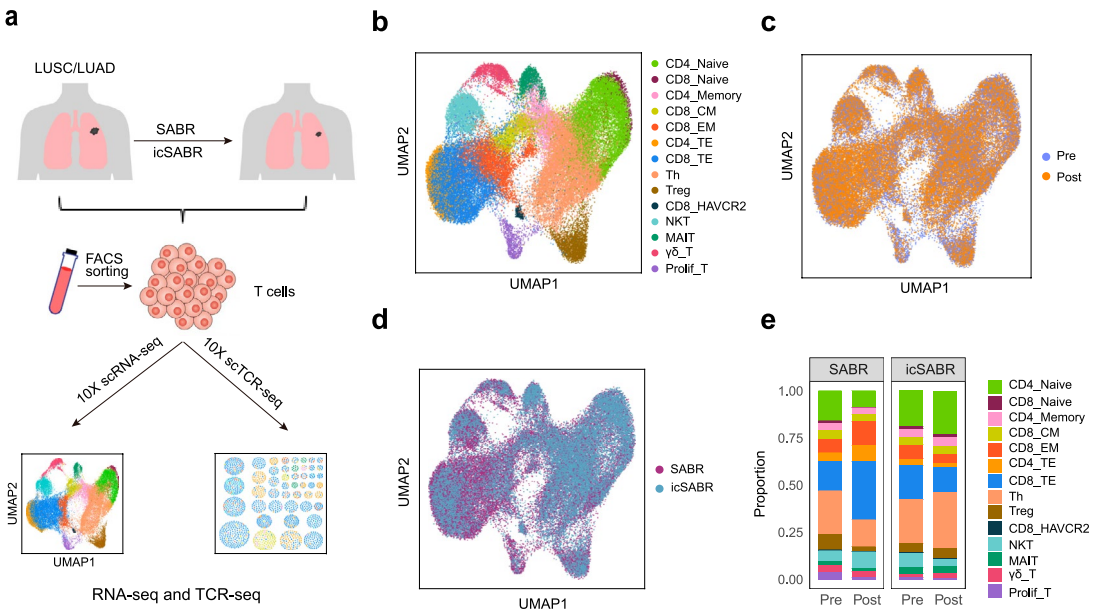
a
LUSC/LUAD
SABR
icSABR
FACS sorting
T cells
10X scRNA-seq
10X scTCR-seq
UMAP2
UMAP1
RNA-seq and TCR-seq
b
UMAP2
UMAP1
CD4_Naive
CD8_Naive
CD4_Memory
CD8_CM
CD8_EM
CD4_TE
CD8_TE
Th
Treg
CD8_HAVCR2
NKT
MAIT
γδ_T
Prolif_T
c
UMAP2
UMAP1
Pre
Post
d
UMAP2
UMAP1
SABR
icSABR
e
SABR
icSABR
Proportion
1.00
0.75
0.50
0.25
0.00
Pre
Post
Pre
Post
CD4_Naive
CD8_Naive
CD4_Memory
CD8_CM
CD8_EM
CD4_TE
CD8_TE
Th
Treg
CD8_HAVCR2
NKT
MAIT
γδ_T
Prolif_T

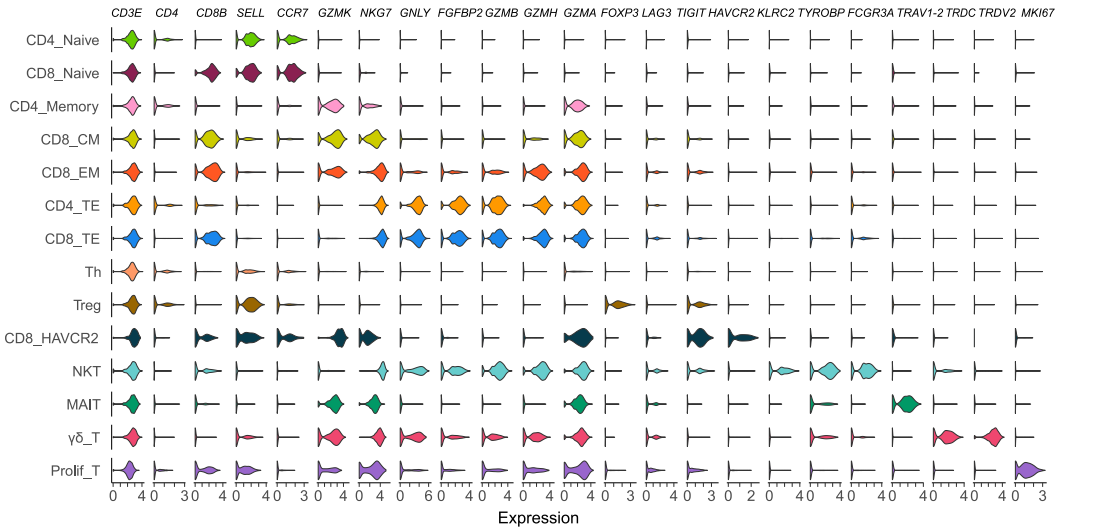
f
CD3E CD4 CD8B SELL CCR7 GZMK NKG7 GNLY FGFBP2 GZMB GZMH GZMA FOXP3 LAG3 TIGIT HAVCR2 KLRC2 TYROBP FCGR3A TRAV1-2 TRDC TRDV2 MKI67
CD4_Naive
CD8_Naive
CD4_Memory
CD8_CM
CD8_EM
CD4_TE
CD8_TE
Th
Treg
CD8_HAVCR2
NKT
MAIT
γδ_T
Prolif_T
Expression

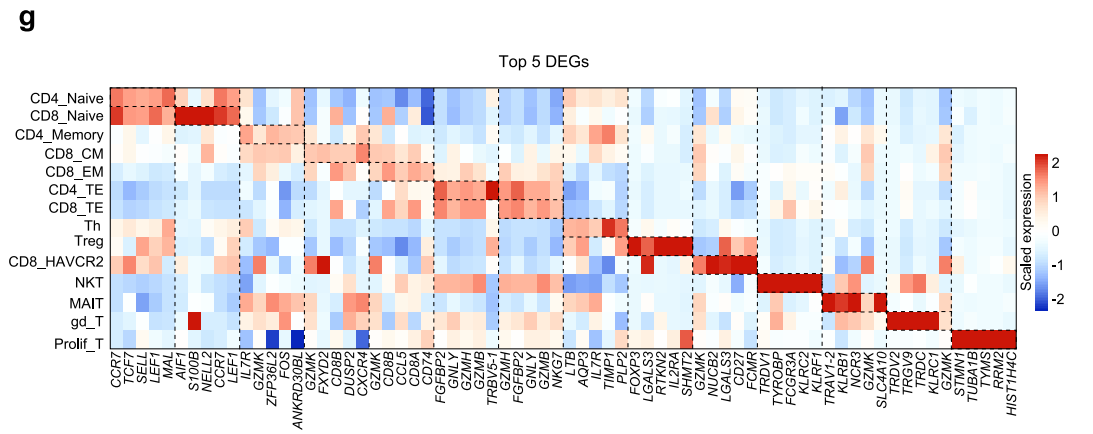
g
Top 5 DEGs
CD4_Naive
CD8_Naive
CD4_Memory
CD8_CM
CD8_EM
CD4_TE
CD8_TE
Th
Treg
CD8_HAVCR2
NKT
MAIT
gd_T
Prolif_T
Scaled expression
2
1
0
-1
-2

◂**Fig. 1** Single-cell transcriptomic analysis of distinct T cell subtypes in the peripheral blood of NSCLC patients who received SABR and icSABR. **a** Schematic of the study design: T cells were isolated from the PBMC of patients before and after SABR ($n=4$) or icSABR ($n=3$) and subjected to single-cell RNA and TCR sequencing, followed by gene expression and clone analysis. **b–d** UMAP plots showing 57,738 T cells, colored by cell clusters (**b**), sampling timepoint (**c,** abbreviated as "Pre" and "Post"), and treatment group (**d,** abbreviated as "icSABR" and "SABR"); each dot corresponds to one cell. **e** Stacked bar chart showing the proportion of total T cells represented by each cluster, categorized by the icSABR and SABR groups. **f** Violin plots showing the expression of the classical marker genes indicating cluster identity. **g** Top five most differentially-expressed genes (DEGs) between the 14 T cell clusters. The colors represent the scaled expression levels, and dot sizes represent the percentage of cells expressing the DEG in the indicated clusters

pre-therapy were performed using *clusterProfiler* package (version 4.4.4) in *R* software software [36]. The plots were generated using *ggplot2* package (version 3.4.2) in *R* software. *P* values < 0.05 were considered statistically significant.

TCR profiling analysis

The *Scirpy* [37] package (version 0.3, implemented in Python) was used to analyze TCR sequencing data. Since the majority of T cells in peripheral blood express T cell receptors composed of two chains, α and β, those instead expressing γ and δ chains were excluded. Then, TCR chains were paired using the "ir.tl.chain_pairing" function, according the tutorial at https://icbi-lab.github.io/scirpy/latest/tutorials. Cells with "No TCR", "Orphan beta", "Orphan alpha", "Two full chains" or "Multichain" were filtered out: only the cells with "Single pair", "Extra alpha" and "Extra beta" chains were retained for further analyses. Clonotypes were identified among T cells based on amino-acid sequence similarity, which was assessed using the "ir.pp.tcr_neighbors" and "ir.tl.define_clonotype_clusters" functions. Clonotypes were then subdivided into "large clones", "small clones" and "single clone", according to the based on how many T cells express identical TCR as defined. When the number of T cells express identical TCR clone greater or equal to 10, they were group into "large clones"; when the number of T cells express identical TCR clone greater than or equal to 2 and less than 10, they were group into "small clones"; when the number of T cells express identical TCR clone equal to 1, they were group into "single clone". Lastly, "ir.tl.repertoire_overlap" function was conducted in order to evaluated the similarity of TCR clonotypes in each cluster. This function could calculate a (Jaccard) distance matrix of clusters as well as the linkage of hierarchical clustering. The distance matrix was shown as a heatmap, while clusters were reordered based on hierarchical clustering.

Reconstructing single-cell denoising and PAGA graph

To denoise the graph, "sc.tl.diffmap" function in *Scanpy* package [38] (version 1.9.3, implemented in Python) was preformed to generate diffusion map space. To quantify the connectivity of clusters within single-cell graph, the PAGA method was used to generate the abstracted graph by preformed "sc.tl.paga" function.

Survival analysis

Bulk RNA-seq data along with the curated clinical information from NSCLC patients post-radiotherapy were sourced from the TCGA database ($n=178$). The high/low cutoffs for expression levels of these marker genes were determined using the survcutpoint function from the survminer R package, and NSCLC patients following radiotherapy were divided into high or low gene expression groups. The log-rank test was performed by the survival package and Kaplan–Meier survival curves were plotted using the ggsurvplot function.

Statistical analysis

All statistical analyses and plots were conducted in R (version 4.2.1) and *Python* (version 3.10.9). Two-sample Wilcoxon rank-sum test was employed to compared significant between involved groups. *P* value < 0.05 was considered statistically significant.

Results

Single-cell transcriptional profiling of peripheral T cells from patients with early-stage NSCLC pre- and post-SABR/icSABR treatment

Our study cohort comprised seven patients with early-stage NSCLC, who generously donated blood samples 1–3 days before and 1–2 months after SABR treatment; four patients were treated with SABR alone, and three were pre-treated with immunotherapy and chemotherapy (icSABR). We first defined the transcriptomic characteristics of T cells from PBMCs using paired blood samples from patients with early-stage NSCLC taken 1–3 days pre-SABR and 1–2 months after SABR treatment. We isolated $CD45^+CD3^+$ T cells from fresh PBMC and subjected them to scRNA-seq using the 10X Genomics Chromium Single Cell platform (Fig. 1a). After quality control, we finally analyzed 57,738 T cells, with an average of 1,352 expressed genes and 3,946 UMIs detected in each (Fig. S1a–c).

We identified fourteen T cell subtypes using unsupervised): naïve T cells (CD4_Naive, CD8_Naive), central

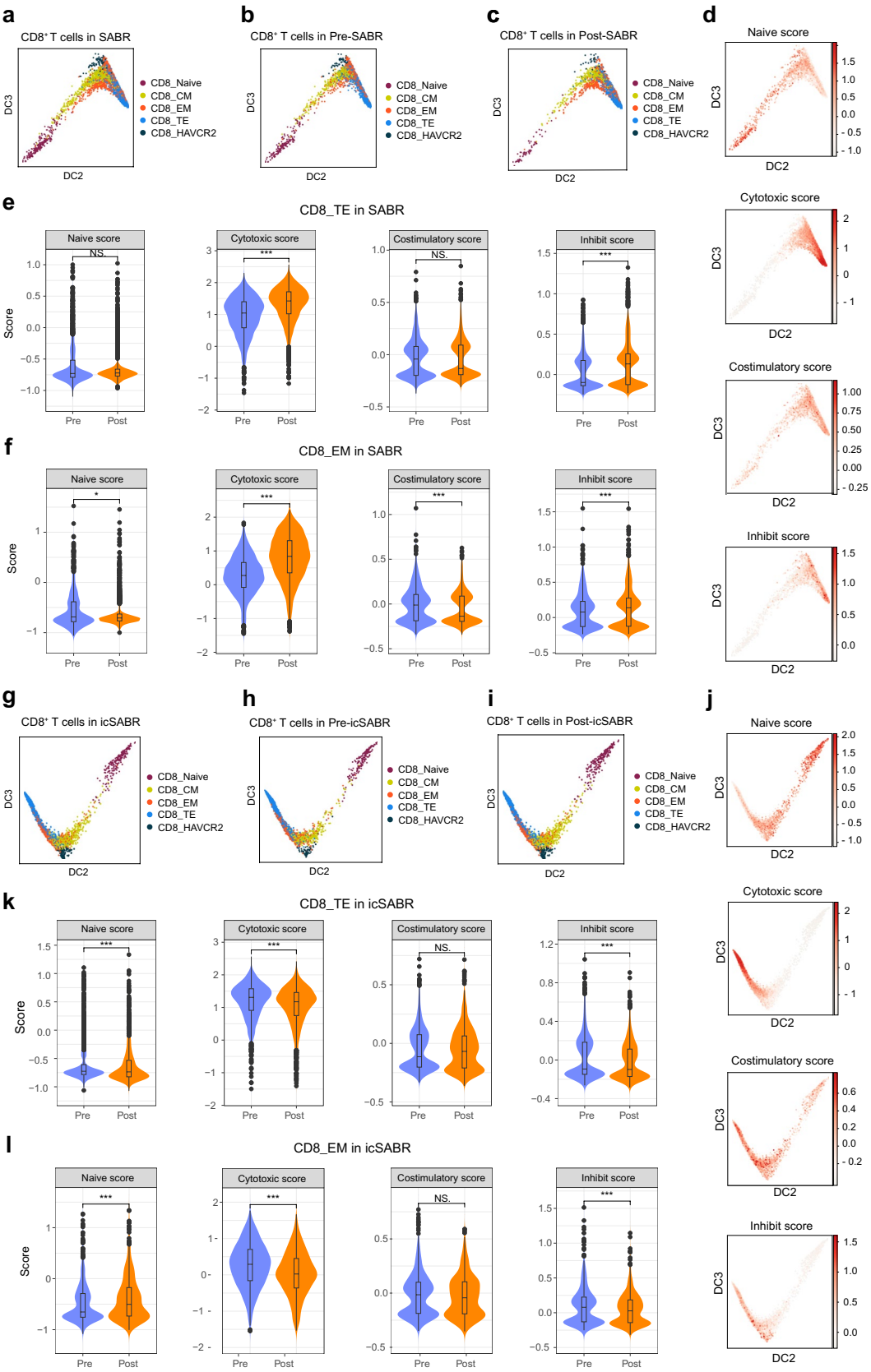
a
CD8⁺ T cells in SABR
b
CD8⁺ T cells in Pre-SABR
c
CD8⁺ T cells in Post-SABR
d
Naive score
CD8_Naive
CD8_CM
CD8_EM
CD8_TE
CD8_HAVCR2
DC3
DC2
e
CD8_TE in SABR
Naive score
Cytotoxic score
Costimulatory score
Inhibit score
Score
NS.
Pre
Post
Cytotoxic score
Costimulatory score
Inhibit score
f
CD8_EM in SABR
g
CD8⁺ T cells in icSABR
h
CD8⁺ T cells in Pre-icSABR
i
CD8⁺ T cells in Post-icSABR
j
Naive score
k
CD8_TE in icSABR
l
CD8_EM in icSABR

◂**Fig. 2** CD8$^+$ T cell functional scores under SABR and icSABR treatment at single-cell resolution. **a–c** Partition-based graph abstraction (PAGA) analysis of CD8$^+$ T cells inferred by Scanpy in SABR group (**a**), pre-SABR (**b**), and post-SABR (**c**). Each dot corresponds to one cell and is colored according to T cell cluster. **d** Naïve, cytotoxic, costimulatory, and inhibitory scores were evaluated in CD8$^+$ T cell subclusters in the SABR group. Intensity of color indicates scaled score levels. **e–f** Changes in naïve, cytotoxic, costimulatory, and inhibitory scores in CD8_TE (**e**) and CD8_EM (**f**) induced by SABR. **g–i** PAGA analysis of CD8$^+$ T cells inferred by Scanpy in icSABR group (**g**), pre-icSABR (**h**), and post-icSABR (**i**). **j** Naïve, cytotoxic, costimulatory, and inhibitory scores were evaluated in CD8$^+$ T cell subclusters in the icSABR group. **k–l** Changes in naïve, cytotoxic, costimulatory, and inhibitory scores in CD8_TE (**k**) and CD8_EM (**l**) induced by icSABR. Data from pre- and post-treatment groups were compared by two-sided Wilcoxon rank-sum test. *$P < 0.05$; **$P < 0.01$; ***$P < 0.001$; NS, not significant

and effector memory T cells (CD4_Memory, CD8_CM, CD8_EM), terminal effector T cells (CD4_TE, CD8_TE), T helper cells (Th), regulatory T cells (Treg), dysfunctional/exhausted T cells (CD8_HAVCR2), natural killer T cells (NKT), mucosal-associated invariant T cells (MAIT), γδ T cells (γδ T) and proliferative T cells (Prolif_T) (Fig. 1b–e). Based on published data, we used a panel of marker genes whose expression identified distinct cell clusters and *SingleR* analysis (Fig. 1f, Fig. S2a–e, Fig. S3a–b): *SELL* and *CCR7* expression marked naïve T cells (both CD4_Naïve and CD8_Naïve subtypes) [39]; while the cluster of cells with high expression of the proliferative gene *MKI67* and G2/M cell cycle was identified as Prolif_T, showing a decrease in cell percentage following SABR (Fig. 1e, Fig. S2c–d). Exhausted/inhibitory markers, including *HAVCR2, TIGIT, PDCD1, LAG3*, and *CTLA4*, were used to identify dysfunctional/exhausted CD8$^+$ T cells (CD8_HAVCR2) (Fig. 1f, Fig. S2a, Fig. S3a–b) [40, 41], while differential expression of *GZMH* distinguished CD8_EM and CD8_CM cells [42]. The two effector clusters including CD4_TE and CD8_TE cells were characterized by high expression of cytotoxicity markers including *GZMH*, *FGFBP2*, *GNLY*, and *NKG7*, and almost no expression of exhaustion marker genes such as *LAG3*, *TIGIT* and *HAVCR2* (Fig. 1f) [43]. We validated the features of CD8_TE cells with high expression of GZMB and low expression of LAG3 (CD223) by flow cytometry (Fig. S2e). Alongside expression of these defining marker genes, each T cell subcluster exhibited distinct gene expression profiles (Fig. 1g, Supplementary Table 3).

Transcriptional changes of CD8$^+$ T cells induced by SABR/icSABR

Having defined the composition of T cell subpopulations in peripheral blood before and after SABR/icSABR, we next conducted an in-depth comparative analysis based on the transcriptional characteristics of these T cell subtypes before and after treatment, and between treatment groups. We first calculated naïve, cytotoxic, costimulatory, inhibitory and Treg feature gene expression scores for each T cell subtype (Fig. S3a–b). Notably, CD8_TE, CD8_EM, CD4_TE, and NKT showed high cytotoxicity scores and low naïve scores, while the CD8_HAVCR2 cell cluster had a relatively high inhibitory score, and—validating the approach—Treg cells had a relatively high Treg score (Fig. S3b). Then, by comparing all T cells between pre- and post-SABR/icSABR, we found that cytotoxic and inhibitory scores were significantly increased after treatment with SABR alone, while they were decreased when SABR was preceded by immunotherapy and chemotherapy (Fig. S3c).

We then began looking at individual T cell subpopulations in more detail, starting with CD8$^+$ T cells. To investigate the transcriptional changes among CD8$^+$ T cell subtypes with potential anti-tumor cytotoxic features, we applied partition-based graph abstraction (PAGA) analysis to construct the likely developmental trajectories of CD8$^+$ T cell subclusters. This suggested that CD8_TE and CD8_EM with high cytotoxic scores and low naïve scores were differentiated from CD8_Naïve in the SABR group and both pre- and post-treatment timepoints (Fig. 2a–d). Thus, we focused on the transcriptional changes in CD8_TE and CD8_EM. By comparing the gene set scores pre- and post-SABR, we found that both cytotoxic and inhibitory scores were significantly elevated in both CD8_TE and CD8_EM (both $P < 0.001$, Fig. 2e–f, Fig.S4a). Moreover, eight new patients with early-stage NSCLC who received SABR alone were included in the validation cohort. And increased proportional change of circulating CD8_TE cells induced by SABR was confirmed using flow cytometry (Fig. S4b–c). Besides, we were able to extend our observations to renal cell carcinoma, where similar findings regarding CD8_TE induced by SABR were noted (Fig. S4d–4j.)

Interestingly, in the icSABR group, we observed a different effect of treatment: while the inferred developmental trajectory of CD8 subtypes was similar to that in the SABR group (Fig. 2g–j), the comparison of feature gene score revealed a relative decrease in the expression of both cytotoxicity-associated and inhibitory genes in both CD8_TE and CD8_EM (all $P < 0.001$, Fig. 2k–l, Fig.S4a). Similarly, when we extended the comparison to NKT and Prolif_T cells, we found that cytotoxic scores were increased after SABR (all $P < 0.001$, Fig. S5a–d) and had a tendency to decrease after icSABR (Fig. S5a–d). Moreover, further analysis of DEGs in Prolif_T cells post- and pre-SABR revealed the upregulating expression levels of *KLF2*, *IFITM1*, and *IFITM2*. GSEA indicated enrichment in the pathways associated with chemokine receptors binding to chemokines and interferon alpha/beta signaling following SABR (Fig. S6a, c). However, following icSABR, the Prolif_T cells exhibited elevated expression levels of *MALAT1* and *AHANK*, and

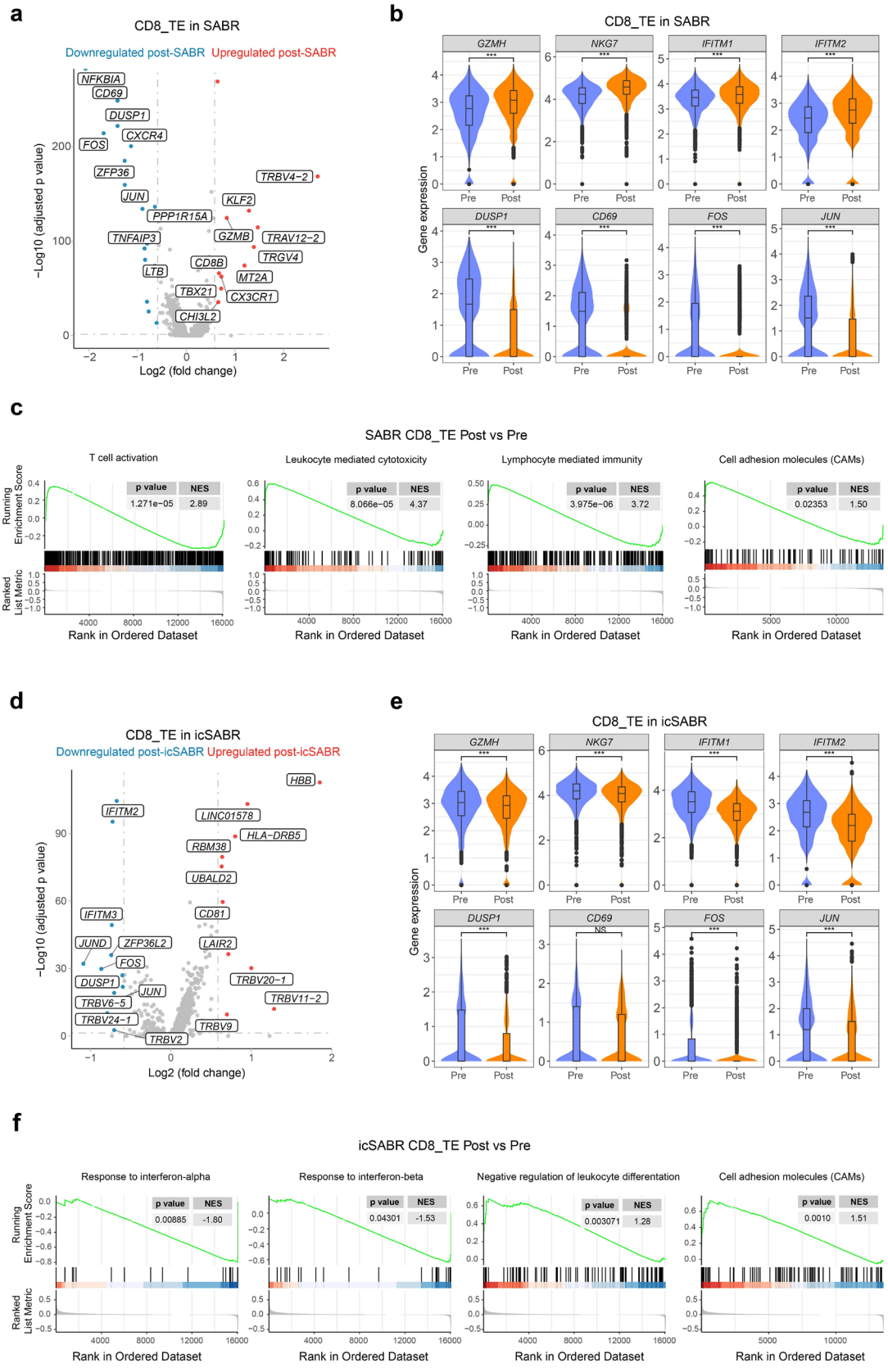
a
CD8_TE in SABR
Downregulated post-SABR Upregulated post-SABR
−Log10 (adjusted p value)
Log2 (fold change)
NFKBIA
CD69
DUSP1
CXCR4
FOS
ZFP36
JUN
PPP1R15A
TNFAIP3
LTB
CD8B
TBX21
CHI3L2
TRBV4−2
KLF2
GZMB
TRAV12−2
TRGV4
MT2A
CX3CR1
b
CD8_TE in SABR
GZMH
NKG7
IFITM1
IFITM2
DUSP1
CD69
FOS
JUN
Gene expression
Pre
Post
c
SABR CD8_TE Post vs Pre
T cell activation
Leukocyte mediated cytotoxicity
Lymphocyte mediated immunity
Cell adhesion molecules (CAMs)
p value
NES
1.271e−05
2.89
8.066e−05
4.37
3.975e−06
3.72
0.02353
1.50
Running Enrichment Score
Ranked List Metric
Rank in Ordered Dataset
d
CD8_TE in icSABR
Downregulated post-icSABR Upregulated post-icSABR
−Log10 (adjusted p value)
Log2 (fold change)
HBB
IFITM2
LINC01578
HLA−DRB5
RBM38
UBALD2
IFITM3
CD81
JUND
ZFP36L2
LAIR2
FOS
DUSP1
JUN
TRBV20−1
TRBV11−2
TRBV6−5
TRBV24−1
TRBV9
TRBV2
e
CD8_TE in icSABR
GZMH
NKG7
IFITM1
IFITM2
DUSP1
CD69
FOS
JUN
NS
Gene expression
Pre
Post
f
icSABR CD8_TE Post vs Pre
Response to interferon-alpha
Response to interferon-beta
Negative regulation of leukocyte differentation
Cell adhesion molecules (CAMs)
p value
NES
0.00885
-1.80
0.04301
-1.53
0.003071
1.28
0.0010
1.51
Running Enrichment Score
Ranked List Metric
Rank in Ordered Dataset

◂**Fig. 3** Transcriptomic changes in CD8_TE cells pre- and post-SABR and icSABR. **a/d** Volcano plot shows DEGs between pre- and post-SABR (**a**)/icSABR (**d**) CD8_TE cells. DEGs upregulated and downregulated in post-SABR/icSABR cells are shown in red and navy blue, respectively. The top ten most significant DEGs are labeled in the plots. **b/e** Violin plots showing the expression level of pathway-related genes compared between post- and pre-SABR (**b**)/icSABR (**e**) CD8_TE cells. Data were compared by two-sided Wilcoxon rank-sum test. $*P<0.05$; $**P<0.01$; $***P<0.001$; NS, not significant. **c/f** GSEA plots showing the enrichment score for selected pathways compared between post- and pre-SABR (**c**)/icSABR (**f**) CD8_TE cells

downregulating pathways related to cell killing, response to cytokine, and leukocyte mediated cytotoxicity (Fig. S6b, d).

Transcriptomic response of CD8_TE to SABR and icSABR

Considering the significant change in feature gene expression among CD8_TE cells, and their key role in tumor control [44], we further investigated their transcriptional response to SABR and icSABR. We compared the transcriptomes of the CD8_TE cluster in samples collected before and after SABR. Our findings revealed an upregulation of genes linked to cytotoxicity, specifically *GZMH*, *NKG7*, *IFITM1*, and *IFITM2*, alongside a downregulation of genes associated with lymphocyte activation, including *DUSP1*, *FOS*, and *JUN*, following SABR treatment (all *P* value < 0.001, Fig. 3a–b, Supplementary Table 4). For comparisons of CD8_TE between pre- and post-SABR, we performed pathway enrichment and found that T cell activation, lymphocyte-mediated cytotoxicity, lymphocyte-mediated immunity, and cell adhesion molecules were significantly enriched after SABR (Fig. 3c, Fig. S7a). Similar results were revealed by the scRNA-seq data from human renal cell carcinoma patients treated with SABR (Fig. S7b).

We then extended our detailed analysis to CD8_TE in pre- and post-icSABR samples (Fig. 3d, Supplementary Table 4). Interestingly, the expression levels of *GZMH*, *NKG7*, *IFITM1*, and *IFITM2* were significantly reduced following icSABR (all $P<0.001$, Fig. 3e), which contrasted with the finding observed in the SABR group. Additionally, the expression of *DUSP1*, *FOS,* and *JUN* also exhibited a decline post-icSABR (all $P<0.001$, Fig. 3e), consistent with the results obtained in the SABR group. Furthermore, those genes involved in response to interferon-α/β signaling and leukocyte differentiation were significantly downregulated after icSABR, which was the opposite to the T cell activation effect in SABR group; while cell adhesion molecules stayed higher after icSABR (Fig. 3f). In order to explore the factors associated with survival following radiotherapy for NSCLC, we conducted survival analysis in the TCGA-NSCLC cohort ($n=178$). Our findings revealed that the genes *FGFBP2* and *S1PR5*, which show high expression in CD8_TE population, were significantly and positively associated with progression-free survival ($P=0.003$ and 0.01, respectively; Fig. S7c).

Transcriptomic response of CD4$^+$ T cells to SABR and icSABR

Moving our focus to CD4$^+$ T cells, we then applied PAGA analysis to construct the potential developmental trajectories of five CD4$^+$ subtypes and found that CD4_TE and Treg cells with high cytotoxic scores and Treg scores, respectively, were differentiated from CD4$^+$ naïve cells in samples from the SABR group (Fig. 4a–d). Then, we focused on the transcriptional differences in CD4_TE and Treg cells before and after SABR, finding that CD4_TE exhibited increased cytotoxic scores and inhibitory scores (all $P<0.001$; Fig. 4e and Fig. S8a), while Treg cells showed decreased inhibitory and Treg scores ($P<0.001$ and <0.01, respectively) after SABR (Fig. 4f). In addition, flow cytometry in the validation cohort confirmed that SABR induced a decrease in proportion of CD4$^+$ Treg cells ($P=0.0027$; Fig. S8b–c).

Concerning the CD4$^+$ T cell subtypes in the icSABR group, developmental trajectories and gene scores of these clusters showed similar results to the SABR group (Fig. 4g–j), as did Treg cells which showed decreased inhibitory scores ($P<0.01$, Fig. 4k–l). However, CD4_TE exhibited decreased cytotoxic scores and inhibitory scores following icSABR (all $P<0.001$, Fig. 4k–l and Fig. S8a), which is the opposite pattern observed after SABR alone.

Single-cell TCR profiling change of T cells induced by SABR/icSABR

Since TCR are often used as unique identifiers of T cell ancestries, we also acquired single-cell TCR-seq data to enable us to track the lineage of each single T cell based on their full-length TCR α and β sequences (Fig. S9a, Supplementary Table 5). By comparing the TCR chains of T cells pre- and post-SABR/icSABR, we found TCR rearrangement after treatment in both groups (Fig. S9b–c).

To further investigate the impact of SABR/icSABR on the clonality of T cells, we divided TCR clones into three groups, according to their size: large clones (clone size ≥ 10), small clones (clone size = 2–9), and single clone (clone size = 1) (Fig. S10a). In the SABR group, the proportion of large clones was higher following SABR, which was accompanied by a decrease in the proportion of single clone (Fig. 5a–c, Fig. S10b). We further clarified that CD8_TE, CD8_EM, CD8_CM, CD4_TE, NKT and Prolif_T were the main cell populations contributing to this alteration (Fig. 5d). Conversely, in the icSABR cohort, the treatment resulted in a decrease in the proportion of large clones and an increase in single clone (Fig. 5e–g, Fig. S10b). The

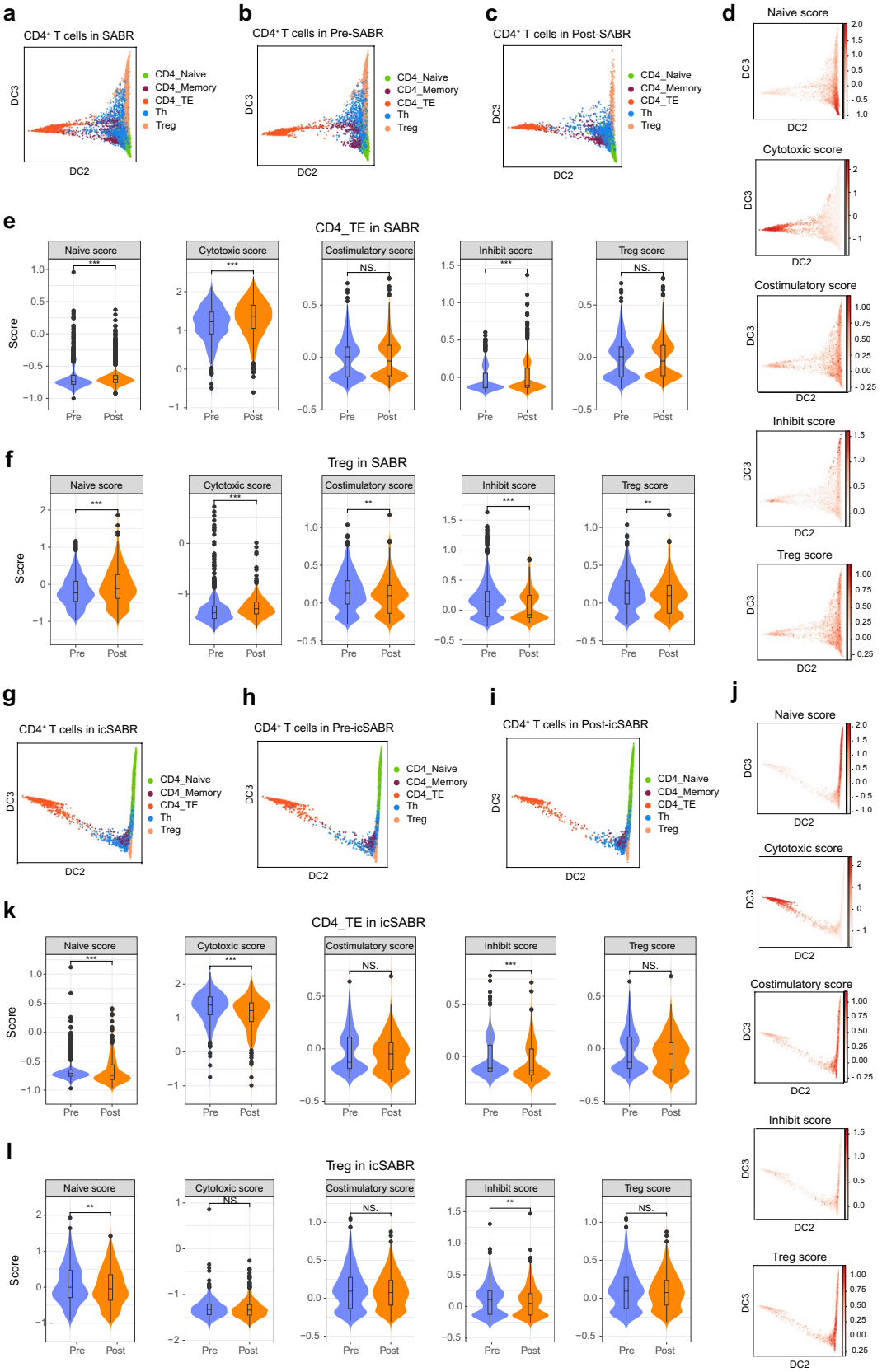
a
CD4⁺ T cells in SABR
b
CD4⁺ T cells in Pre-SABR
c
CD4⁺ T cells in Post-SABR
CD4_Naive
CD4_Memory
CD4_TE
Th
Treg
DC3
DC2
d
Naive score
Cytotoxic score
Costimulatory score
Inhibit score
Treg score
e
CD4_TE in SABR
f
Treg in SABR
Score
Pre
Post
NS.
g
CD4⁺ T cells in icSABR
h
CD4⁺ T cells in Pre-icSABR
i
CD4⁺ T cells in Post-icSABR
j
k
CD4_TE in icSABR
l
Treg in icSABR

◂**Fig. 4** $CD4^+$ T cell functional scores under SABR and icSABR at single-cell resolution. **a–c** PAGA analysis of $CD4^+$ T cells in SABR group (**a**), pre-SABR (**b**), and post-SABR (**c**). Each dot corresponds to one cell and is colored according to T cell cluster; black arrows indicate the T cell development directions predicted by functional scores. **d** Naïve, cytotoxic, costimulatory, inhibitory and Treg scores were evaluated in $CD4^+$ T cell subclusters in SABR group. Intensity of color indicates scaled score levels. **e–f** Changes in naïve, cytotoxic, costimulatory, inhibitory and Treg scores in CD4_TE (**e**) and Treg cells (**f**) induced by SABR. **g–i** PAGA analysis of $CD4^+$ T cells in icSABR group (**g**), pre-icSABR (**h**), and post-icSABR (**i**). **j** Naïve, cytotoxic, costimulatory, inhibitory and Treg scores were evaluated in $CD4^+$ T cell subclusters in icSABR group. **k–l** Changes in naïve, cytotoxic, costimulatory, inhibitory and Treg scores in CD4_TE (**k**) and Treg cells (**l**) induced by icSABR. Data from pre- and post-treatment groups were compared by two-sided Wilcoxon rank-sum test. $^*P<0.05$; $^{**}P<0.01$; $^{***}P<0.001$; NS, not significant

same cell populations—CD8_TE, CD8_EM, CD8_CM, CD4_TE, and NKT—were identified as the key contributors to this observed change (Fig. 5h). Notably, these T cell subtypes exhibited TCR overlap before and after SABR or icSABR (Fig. 5i–j), which further highlights their possible relevance in early-stage NSCLC patients treated with SABR or icSABR.

Changed TCR clonotypes post-SABR/icSABR at single-cell resolution

Comparing the clonotypes pre-SABR we found 3380 distinct TCR clonotypes post-SABR, with only 373 clonotypes shared between the pre- and post-SABR samples (Fig. 6a). After SABR, 3380 different TCR clonotypes were mainly the large and single clones, and predominantly from CD8_TE cells (Fig. 6b). We further showed the details of T cell subclusters with large clones before and after SABR (Fig. 6c). When we compared the transcriptomes of CD8_TE cells between the single, small and large clones post-SABR, we found high expression of *GZMB* and *NKG7* in cells with large clones, and *GZMK*, *IL7R*, and *SELL* in small and single clones (Fig. 6d, Supplementary Table 6). This suggested that T cells after SABR with large clones may have higher cytotoxicity than those with small and single clones.

In samples from the icSABR group, we identified 7644 distinct TCR clonotypes following icSABR, with only 366 clonotypes overlapped with the pre-treatment samples (Fig. 6e). Interestingly, different from the SABR-only treatment group, clonotypes post-icSABR were mainly single clone but not large clone, and they were mainly from Th cells (Fig. 6f). Also, the details of T cell subclusters with large clones before and after icSABR were showed (Fig. 6g). Then, we investigated the DEGs between CD8_TE in the large, small, and single clones post-icSABR, and found high expression of *GZMB* in cells with large clones, and of *IL7R*, *SELL*, and *GZMK* in single clones (Fig. 6h, Supplementary Table 6).

Discussion

Here, we have provided a high-resolution transcriptomic depiction of T cell diversity pre- and post-SABR/icSABR, identifying fourteen T cell subclusters with distinct transcriptional and clonal features that were presented in the peripheral blood of patients with NSCLC. Our study reported two distinct patterns of peripheral T cell response induced by SABR and icSABR, which could have profound implications for the design of more rational treatment approaches and regimens for early-stage NSCLC.

Among these subclusters, CD8_TE showed increased cytotoxic and inhibitory feature gene expression scores after SABR, while the opposite effect was seen in the group treated with icSABR. Pathway enrichment analyses of CD8_TE also showed that T cell activation and lymphocyte-mediated cytotoxicity were enriched post-SABR but not icSABR. In addition, interferon-α/β signalings were downregulated after icSABR. Researchers found that $CD39^+CD103^+CD8^+$ tumor-infiltrating T cells (TILs) with selective reactivity to autologous tumor cells and enhanced cytotoxicity also expressed high levels of inhibition markers (PD-1, CTLA-4 and TIM-3) [45]. Moreover, $CD8^+$ TILs with empirically validated tumor reactivity were all marked by expression of PDCD1, ENTPD1 and CXCL13 which were generally considered to be markers of $CD8^+$ T cell exhaustion [46, 47]. And $CD8^+$ TILs obtained from patient tissues with enrichment for transcriptional signature of T cell dysfunction were demonstrated reactivity against autologous tumor [48]. Notably, a high early on-treatment abundance of $CD8^+$ TILs expressing exhaustion markers (such as PD-1, CD39, and CTLA4) is predictive of a clinical benefit from immunotherapy across tumor type [49, 50]. In light of these findings, $CD8^+$ T cells expressing high cytotoxicity/ inhibition markers are enriched for tumor-reactive clones and predict clinical benefit from immunotherapy. Thus, we suggested that icSABR showed less benefit than SABR in terms of T cell activation. These data may explain earlier observations made by Wei et al. [51] in tumor-bearing mice, which suggested that administration of anti-PD-1 before irradiation abrogated systemic immunity by the reduction of polyfunctional effector $CD8^+$ T cells at the irradiated tumor site, potentially leading to a suboptimal systemic anti-tumor response at abscopal sites. Thus, we provide the first data in humans that—as in mouse models—administration of immune-checkpoint inhibitor therapy prior to SABR, while intuitively indicated, may not be the optimal approach in all settings.

A similar enhanced immune response following SABR has also been observed in $CD4^+$ T cells and proliferating T cells. We found increased cytotoxic scores in CD4_TE

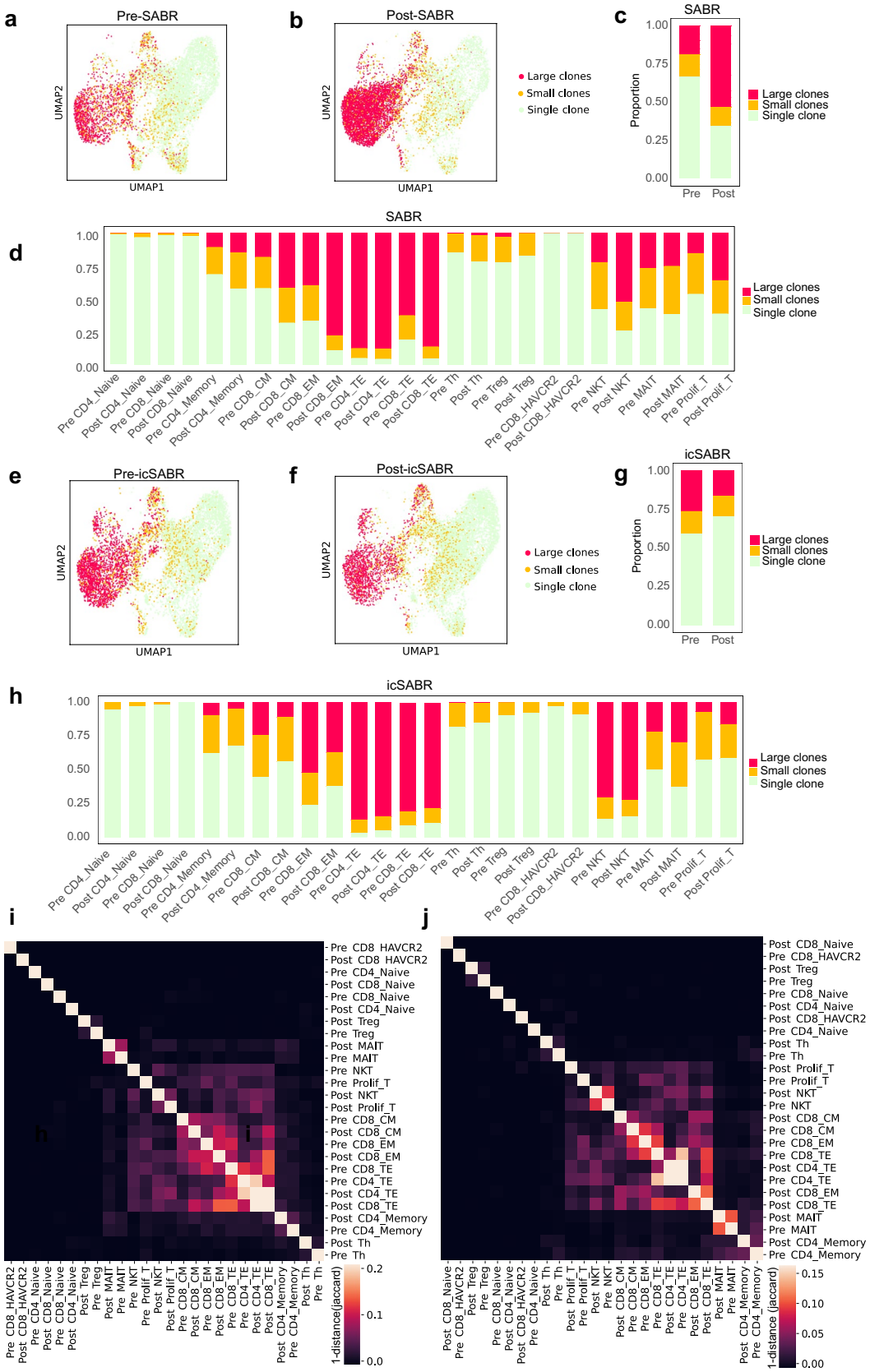
a
Pre-SABR
UMAP2
UMAP1
b
Post-SABR
UMAP2
UMAP1
Large clones
Small clones
Single clone
c
SABR
Proportion
1.00
0.75
0.50
0.25
0.00
Pre
Post
Large clones
Small clones
Single clone
d
SABR
1.00
0.75
0.50
0.25
0.00
Pre CD4_Naive
Post CD4_Naive
Pre CD8_Naive
Post CD8_Naive
Pre CD4_Memory
Post CD4_Memory
Pre CD8_CM
Post CD8_CM
Pre CD8_EM
Post CD8_EM
Pre CD4_TE
Post CD4_TE
Pre CD8_TE
Post CD8_TE
Pre Th
Post Th
Pre Treg
Post Treg
Pre CD8_HAVCR2
Post CD8_HAVCR2
Pre NKT
Post NKT
Pre MAIT
Post MAIT
Pre Prolif_T
Post Prolif_T
Large clones
Small clones
Single clone
e
Pre-icSABR
UMAP2
UMAP1
f
Post-icSABR
UMAP2
UMAP1
Large clones
Small clones
Single clone
g
icSABR
Proportion
1.00
0.75
0.50
0.25
0.00
Pre
Post
Large clones
Small clones
Single clone
h
icSABR
1.00
0.75
0.50
0.25
0.00
Pre CD4_Naive
Post CD4_Naive
Pre CD8_Naive
Post CD8_Naive
Pre CD4_Memory
Post CD4_Memory
Pre CD8_CM
Post CD8_CM
Pre CD8_EM
Post CD8_EM
Pre CD4_TE
Post CD4_TE
Pre CD8_TE
Post CD8_TE
Pre Th
Post Th
Pre Treg
Post Treg
Pre CD8_HAVCR2
Post CD8_HAVCR2
Pre NKT
Post NKT
Pre MAIT
Post MAIT
Pre Prolif_T
Post Prolif_T
Large clones
Small clones
Single clone
i
Pre CD8 HAVCR2
Post CD8 HAVCR2
Pre CD4_Naive
Post CD8_Naive
Pre CD8_Naive
Post CD4_Naive
Post Treg
Pre Treg
Post MAIT
Pre MAIT
Pre NKT
Pre Prolif_T
Post NKT
Post Prolif_T
Pre CD8_CM
Post CD8_CM
Pre CD8_EM
Post CD8_EM
Pre CD8_TE
Pre CD4_TE
Post CD4_TE
Post CD8_TE
Post CD4_Memory
Pre CD4_Memory
Post Th
Pre Th
h
i
1-distance(jaccard)
0.2
0.1
0.0
j
Post CD8_Naive
Pre CD8_HAVCR2
Post Treg
Pre Treg
Pre CD8_Naive
Post CD4_Naive
Post CD8_HAVCR2
Pre CD4_Naive
Post Th
Pre Th
Post Prolif_T
Pre Prolif_T
Post NKT
Pre NKT
Post CD8_CM
Pre CD8_CM
Pre CD8_EM
Post CD8_EM
Pre CD4_TE
Post CD4_TE
Post CD8_TE
Pre CD8_TE
Post MAIT
Pre MAIT
Post CD4_Memory
Pre CD4_Memory
1-distance (jaccard)
0.15
0.10
0.05
0.00

◂**Fig. 5** Comparison of TCR repertoire pre- and post-SABR/icSABR at single-cell resolution. **a–b/e–f** UMAP showing three clonal expansion types of T cells in SABR (**a–b**)/icSABR (**e–f**) groups, separated by pre- and post-therapy. **c/g** Relative proportions of TCR clonal expansion types in pre- and post-SABR (**c**)/icSABR (**g**) groups. **d/h** Stacked bar chart demonstrating the proportion of TCR clonal expansion types within each T cell cluster in pre- and post-SABR (**d**)/icSABR (**h**) groups. **i/j** Heatmap showing the Jaccard-index among the T cell subclusters in pre- and post-SABR (**i**)/icSABR (**j**) groups. Lighter color indicates a greater number of overlapping clonotypes between two corresponding clusters

after SABR; however, the opposite result was noted after icSABR. Specifically, after SABR, Tregs exhibited not only a decrease in cell proportion but also a downregulation of immune inhibitory and Treg scores. This finding is consistent with previous studies indication that SABR stimulates inflammation by increasing the proportion of peripheral $CD4^+$ T cells, $CD8^+$ T cells, and NK cells, while simultaneously decreasing the proportion of Tregs [14, 15]. In terms of proliferating T cells, a prior study found that the pre-existing Ki-67^+CD8^+ T cells increased following SABR, suggesting a synergistic effect of sustained activation of host anti-tumor immunity [52]. In our study, although the percentage of proliferating T cells decreased after SABR, the activity of pathways associated with the anti-tumor immune response was significantly enhanced, including the chemokine receptors binding chemokines pathway and interferon alpha/beta signaling pathway. These results are in line with the previously reported role of SABR in promoting the involvement of proliferating T cells in the immune response [53].

In cancer immunity, the T cell receptor recognizes major histocompatibility complex (MHC)-bound cancer-specific antigens, serving as the first signal to activate cytotoxic T lymphocytes. Formenti et al. explored TCR dynamics in PBMCs from patients with lung cancer undergoing combined treatment with SABR and CTLA-4 blockade. They found that some TCR clonotypes expanded while others contracted in patients whose cancer responded well to treatment, whereas little change was observed in non-responders or those with stable disease [54]. Li et al. revealed that the TCRs of PBMCs exhibited greater diversity before concurrent chemoradiotherapy (CCRT) than after CCRT in cervical cancer. In tumor tissues, TCR diversity increased slightly three weeks after the initiation of CCRT but subsequently declined by the end of treatment [55]. However, these studies employed bulk sequencing and, as a result, could not evaluate the effects of radiotherapy with or without immunotherapy upon the TCR repertoire among individual T cells.

In our study, the most noticeable effect of SABR on TCRs was the alteration of clone size, characterized by a significant increase in large clones following SABR. However, the addition of prior immunotherapy and chemotherapy to SABR resulted in a decrease in the prevalence of large clones and an increase in the occurrence of single clone, suggesting that prior immunotherapy and chemotherapy influence the impact of SABR on TCRs. The alteration of TCR clones in icSABR group is probably associated with nonideal tumor-reactive TCR clonotypes. One possible explanation for this observation is that highly activated and proliferative T cells, induced by prior immunotherapy is hard for further activation with the release of tumor-related neoantigens induced by SABR. This is consistent with the 'decreasing potential' model of T cells [56]. The reduction in large clones and the suboptimal molecular profile of peripheral T cells all indicate a hypofunctional T cell state during icSABR. The sequence of immunotherapy and SABR may partially elucidate the efficacy of this combination treatment. Compared with receiving stereotactic radiosurgery after ipilimumab, previous studies of patients with melanoma brain metastases have shown that stereotactic radiosurgery administered during or before ipilimumab is associated with favorable local control and overall survival [57]. Our data underscore the necessity for a more comprehensive understanding of SABR in the context of prior anti-PD-1 treatment, with the objective of improving current immunotherapy strategies and ultimately achieving tumor eradication.

When we looked at which cell types were contributing to these clones, we identified CD8_TE, CD8_EM, CD8_CM, CD4_TE, and NKT cells as key players. Among these, the mature T cell types (CD4/CD8_TE and CD8_EM) have a higher proportion of large clones. Our results support the general consensus that radiotherapy helps to generate the diverse TCR repertoire required to achieve tumor rejection [58], and revealed key T cell subclusters that may be responsible for the synergy between radiotherapy and immunotherapy. A previous study conducted on breast cancer mouse models showed that radiation treatment increased the diversity of TCR in tumor-infiltrating T cells, even in the presence of immunotherapy [59]. Here, we show that both SABR and icSABR change TCR clonotypes in peripheral blood T cell populations. Interestingly, icSABR induced more different clonotypes than did SABR. Performing differential-expression analysis on large clones versus all others in CD8_TE revealed that CD8_TE with large clones highly express genes implicated in cytotoxicity that are characteristic of effector T cells. Together with the increased cross-presentation of tumor-derived antigens induced by radiation [60], TCR remodeling can result in a broadening of the anti-tumor immune response.

Taken together, our data provide important novel insight into the distinct patterns of systemic immune activation in patients receiving SABR or icSABR at the single-cell level. SABR showed more benefits than icSABR in terms of T cell activation and the increase of large clones, suggesting that SABR may induce a more robust anti-tumor immune

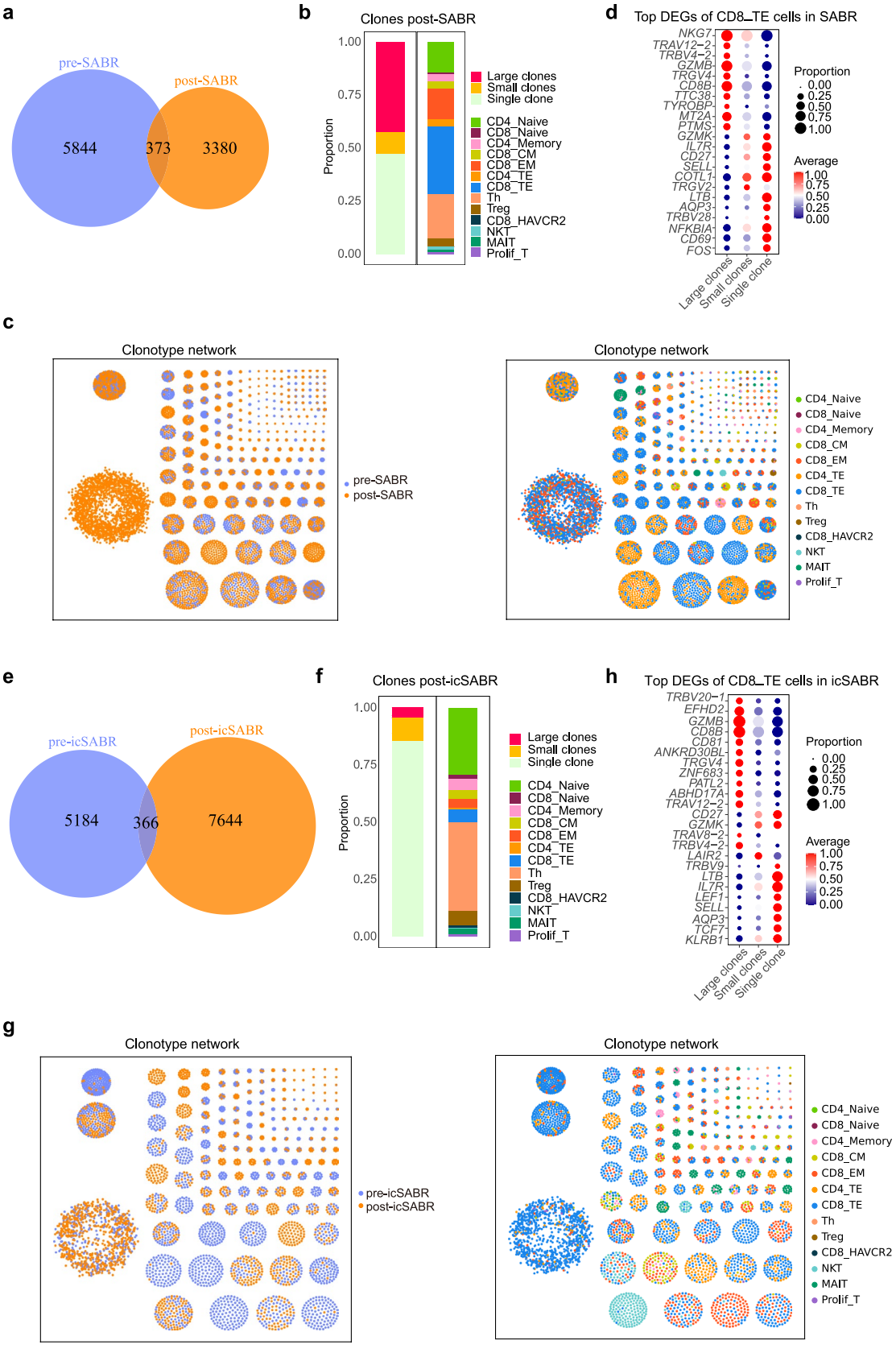
a
pre-SABR
post-SABR
5844
373
3380
b
Clones post-SABR
Proportion
1.00
0.75
0.50
0.25
0.00
Large clones
Small clones
Single clone
CD4_Naive
CD8_Naive
CD4_Memory
CD8_CM
CD8_EM
CD4_TE
CD8_TE
Th
Treg
CD8_HAVCR2
NKT
MAIT
Prolif_T
d
Top DEGs of CD8_TE cells in SABR
NKG7
TRAV12−2
TRBV4−2
GZMB
TRGV4
CD8B
TTC38
TYROBP
MT2A
PTMS
GZMK
IL7R
CD27
SELL
COTL1
TRGV2
LTB
AQP3
TRBV28
NFKBIA
CD69
FOS
Large clones
Small clones
Single clone
Proportion
0.00
0.25
0.50
0.75
1.00
Average
1.00
0.75
0.50
0.25
0.00
c
Clonotype network
pre-SABR
post-SABR
Clonotype network
CD4_Naive
CD8_Naive
CD4_Memory
CD8_CM
CD8_EM
CD4_TE
CD8_TE
Th
Treg
CD8_HAVCR2
NKT
MAIT
Prolif_T
e
pre-icSABR
post-icSABR
5184
366
7644
f
Clones post-icSABR
Proportion
1.00
0.75
0.50
0.25
0.00
Large clones
Small clones
Single clone
CD4_Naive
CD8_Naive
CD4_Memory
CD8_CM
CD8_EM
CD4_TE
CD8_TE
Th
Treg
CD8_HAVCR2
NKT
MAIT
Prolif_T
h
Top DEGs of CD8_TE cells in icSABR
TRBV20−1
EFHD2
GZMB
CD8B
CD81
ANKRD30BL
TRGV4
ZNF683
PATL2
ABHD17A
TRAV12−2
CD27
GZMK
TRAV8−2
TRBV4−2
LAIR2
TRBV9
LTB
IL7R
LEF1
SELL
AQP3
TCF7
KLRB1
Large clones
Small clones
Single clone
Proportion
0.00
0.25
0.50
0.75
1.00
Average
1.00
0.75
0.50
0.25
0.00
g
Clonotype network
pre-icSABR
post-icSABR
Clonotype network
CD4_Naive
CD8_Naive
CD4_Memory
CD8_CM
CD8_EM
CD4_TE
CD8_TE
Th
Treg
CD8_HAVCR2
NKT
MAIT
Prolif_T

◂**Fig. 6** Clonotype analysis of T cell clusters pre- and post-SABR/icSABR. **a/e** Venn diagram showing the number of clonotypes in pre- and post-SABR (**a**)/icSABR (**e**) samples. **b/f** Stacked bar chart showing proportion of clonal expansion types and T cell subclusters with different TCR clonotypes in post-SABR (**b**)/icSABR (**f**) group. **c/g** Networks of the TCR clonotypes with greater than ten cells in SABR (**c**)/icSABR (**g**) groups, colored according to pre- and post-therapy (left panel) and T cell subcluster (right panel). Each dot corresponds to a single cell. Each convergent clonotype cluster represents a subnetwork corresponding to a clonotype cluster defined based on amino acid sequence similarity. **d/h** Dot plots show the top DEGs among the clonal expansion types of CD8_TE in SABR (**d**)/icSABR (**h**) groups. The colors represent the average gene expression levels, and dot sizes represent the number of expressed genes within a cluster

response. To further advance our knowledge, future studies should aim to assess these effects in larger cohorts of patients, with the inclusion of matched tumor tissues, multiple timepoints of blood sampling and long-term clinical follow-up.

Supplementary Information The online version contains supplementary material available at https://doi.org/10.1007/s00262-024-03935-8.

Acknowledgements We wish to thank Dr Lucy Robinson of Insight Editing London for assistance with manuscript preparation.

Author contributions B.S., Z.C.L. and B.L. conceived this study; C.L. collected the samples and performed the experiment; C.L., Y.J.C. and X.H.L. performed the data analysis and wrote the manuscript. Z.J.B., M.L.J., D.S.S., W.X.Z., and R.H. contributed to sample and clinical data collection. Q.Y.H., F.H.W., J.Y.Z. and H.R.S. prepared figures and tables. B.S., Z.C.L. and B.L. jointly supervised this work. All authors have reviewed and approved the final manuscript.

Funding This work was supported by National Key Clinical Specialty Construction Project for Military and Beijing Municipal Natural Science Foundation (No. 7202195), Postdoctoral Fellowship Program of CPSF (grant no. GZB20230041), Shandong Provincial Natural Science Foundation (ZR2021QH006), and National Natural Science Foundation of China (82473315).

Data and code availability The scRNA-seq and TCR-seq datasets in this study have been deposited into the NCBI Gene Expression Omnibus (GEO) database, under accession number GSE190905. Codes used for this study have been uploaded and available at https://github.com/Chenyanjuan1993/Project_NSCLC

Declarations

Conflict of interest The authors declare no competing interests.

References

1. Timmerman R, Paulus R, Galvin J et al (2010) Stereotactic body radiation therapy for inoperable early stage lung cancer. JAMA 303:1070–1076. https://doi.org/10.1001/jama.2010.261
2. Chang JY, Mehran RJ, Feng L et al (2021) Stereotactic ablative radiotherapy for operable stage I non-small-cell lung cancer (revised STARS): long-term results of a single-arm, prospective trial with prespecified comparison to surgery. Lancet Oncol 22:1448–1457. https://doi.org/10.1016/S1470-2045(21)00401-0
3. Chang JY, Senan S, Paul MA et al (2015) Stereotactic ablative radiotherapy versus lobectomy for operable stage I non-small-cell lung cancer: a pooled analysis of two randomised trials. Lancet Oncol 16:630–637. https://doi.org/10.1016/S1470-2045(15)70168-3
4. Videtic GMM, Donington J, Giuliani M et al (2017) Stereotactic body radiation therapy for early-stage non-small cell lung cancer: executive summary of an ASTRO evidence-based guideline. Pract Radiat Oncol 7:295–301. https://doi.org/10.1016/j.prro.2017.04.014
5. Palma D, Visser O, Lagerwaard FJ et al (2010) Impact of introducing stereotactic lung radiotherapy for elderly patients with stage I non-small-cell lung cancer: a population-based time-trend analysis. J Clin Oncol 28:5153–5159. https://doi.org/10.1200/JCO.2010.30.0731
6. Bernstein MB, Krishnan S, Hodge JW et al (2016) Immunotherapy and stereotactic ablative radiotherapy (ISABR): a curative approach? Nat Rev Clin Oncol 13:516–524. https://doi.org/10.1038/nrclinonc.2016.30
7. Brix N, Tiefenthaller A, Anders H et al (2017) Abscopal, immunological effects of radiotherapy: narrowing the gap between clinical and preclinical experiences. Immunol Rev 280:249–279. https://doi.org/10.1111/imr.12573
8. Abuodeh Y, Venkat P, Kim S (2016) Systematic review of case reports on the abscopal effect. Curr Probl Cancer 40:25–37. https://doi.org/10.1016/j.currproblcancer.2015.10.001
9. Herrera FG, Bourhis J, Coukos G (2017) Radiotherapy combination opportunities leveraging immunity for the next oncology practice. CA Cancer J Clin 67:65–85. https://doi.org/10.3322/caac.21358
10. Chen H-M, Ma G, Gildener-Leapman N et al (2015) Myeloid-derived suppressor cells as an immune parameter in patients with concurrent sunitinib and stereotactic body radiotherapy. Clin Cancer Res 21:4073–4085. https://doi.org/10.1158/1078-0432.CCR-14-2742
11. de Goeje PL, Smit EF, Waasdorp C et al (2017) Stereotactic ablative radiotherapy induces peripheral T-cell activation in patients with early-stage lung cancer. Am J Respir Crit Care Med 196:1224–1227. https://doi.org/10.1164/rccm.201610-2178LE
12. Navarro-Martín A, Galiana IL, Berenguer Frances MA et al (2018) Preliminary study of the effect of stereotactic body radiotherapy (SBRT) on the immune system in lung cancer patients unfit for surgery: immunophenotyping analysis. Int J Mol Sci. https://doi.org/10.3390/ijms19123963
13. Trovo M, Giaj-Levra N, Furlan C et al (2016) Stereotactic body radiation therapy and intensity modulated radiation therapy induce different plasmatic cytokine changes in non-small cell lung cancer patients: a pilot study. Clin Transl Oncol 18:1003–1010. https://doi.org/10.1007/s12094-015-1473-x

14. Zhang T, Yu H, Ni C et al (2017) Hypofractionated stereotactic radiation therapy activates the peripheral immune response in operable stage I non-small-cell lung cancer. Sci Rep 7:4866. https://doi.org/10.1038/s41598-017-04978-x
15. McGee HM, Daly ME, Azghadi S et al (2018) Stereotactic ablative radiation therapy induces systemic differences in peripheral blood immunophenotype dependent on irradiated site. Int J Radiat Oncol Biol Phys 101:1259–1270. https://doi.org/10.1016/j.ijrobp.2018.04.038
16. Zhou P, Chen D, Zhu B et al (2020) Stereotactic body radiotherapy is effective in modifying the tumor genome and tumor immune microenvironment in non-small cell lung cancer or Lung metastatic carcinoma. Front Immunol 11:594212. https://doi.org/10.3389/fimmu.2020.594212
17. Chow J, Hoffend NC, Abrams SI et al (2020) Radiation induces dynamic changes to the T cell repertoire in renal cell carcinoma patients. Proc Natl Acad Sci USA 117:23721–23729. https://doi.org/10.1073/pnas.2001933117
18. Tang C, Welsh JW, de Groot P et al (2017) Ipilimumab with stereotactic ablative radiation therapy: phase i results and immunologic correlates from peripheral T cells. Clin Cancer Res 23:1388–1396. https://doi.org/10.1158/1078-0432.CCR-16-1432
19. Postow MA, Callahan MK, Barker CA et al (2012) Immunologic correlates of the abscopal effect in a patient with melanoma. N Engl J Med 366:925–931. https://doi.org/10.1056/NEJMoa1112824
20. Ren X, Zhang L, Zhang Y et al (2021) Insights gained from single-cell analysis of immune cells in the tumor microenvironment. Annu Rev Immunol 39:583–609. https://doi.org/10.1146/annurev-immunol-110519-071134
21. Chow J, Khan A, Gaudieri M et al (2023) Tumor and immune remodeling following radiotherapy in human renal cell carcinoma. J Immunother Cancer. https://doi.org/10.1136/jitc-2022-006392
22. Butler A, Hoffman P, Smibert P et al (2018) Integrating single-cell transcriptomic data across different conditions, technologies, and species. Nat Biotechnol 36:411–420. https://doi.org/10.1038/nbt.4096
23. Stoeckius M, Zheng S, Houck-Loomis B et al (2018) Cell Hashing with barcoded antibodies enables multiplexing and doublet detection for single cell genomics. Genome Biol 19:224. https://doi.org/10.1186/s13059-018-1603-1
24. Stuart T, Butler A, Hoffman P et al (2019) Comprehensive integration of single-cell data. Cell 177:1888–902.e21. https://doi.org/10.1016/j.cell.2019.05.031
25. Macosko EZ, Basu A, Satija R et al (2015) Highly parallel genome-wide expression profiling of individual cells using nanoliter droplets. Cell 161:1202–1214. https://doi.org/10.1016/j.cell.2015.05.002
26. Tirosh I, Izar B, Prakadan SM et al (2016) Dissecting the multicellular ecosystem of metastatic melanoma by single-cell RNA-seq. Science 352:189–196. https://doi.org/10.1126/science.aad0501
27. Aran D, Looney AP, Liu L et al (2019) Reference-based analysis of lung single-cell sequencing reveals a transitional profibrotic macrophage. Nat Immunol 20:163–172. https://doi.org/10.1038/s41590-018-0276-y
28. Mabbott NA, Baillie JK, Brown H et al (2013) An expression atlas of human primary cells: inference of gene function from coexpression networks. BMC Genomics 14:632. https://doi.org/10.1186/1471-2164-14-632
29. Consortium EP (2012) An integrated encyclopedia of DNA elements in the human genome. Nature 489:57–74. https://doi.org/10.1038/nature11247
30. Martens JHA, Stunnenberg HG (2013) BLUEPRINT: mapping human blood cell epigenomes. Haematologica 98:1487–1489. https://doi.org/10.3324/haematol.2013.094243
31. Novershtern N, Subramanian A, Lawton LN et al (2011) Densely interconnected transcriptional circuits control cell states in human hematopoiesis. Cell 144:296–309. https://doi.org/10.1016/j.cell.2011.01.004
32. Azizi E, Carr AJ, Plitas G et al (2018) Single-cell map of diverse immune phenotypes in the breast tumor microenvironment. Cell 174:1293–308.e36. https://doi.org/10.1016/j.cell.2018.05.060
33. Bi K, He MX, Bakouny Z et al (2021) Tumor and immune reprogramming during immunotherapy in advanced renal cell carcinoma. Cancer Cell 39:649–61.e5. https://doi.org/10.1016/j.ccell.2021.02.015
34. Qian J, Olbrecht S, Boeckx B et al (2020) A pan-cancer blueprint of the heterogeneous tumor microenvironment revealed by single-cell profiling. Cell Res 30:745–762. https://doi.org/10.1038/s41422-020-0355-0
35. Sun Y, Wu L, Zhong Y et al (2021) Single-cell landscape of the ecosystem in early-relapse hepatocellular carcinoma. Cell 184:404–21.e16. https://doi.org/10.1016/j.cell.2020.11.041
36. Yu G, Wang LG, Han Y et al (2012) clusterProfiler: an R package for comparing biological themes among gene clusters. OMICS 16:284–287. https://doi.org/10.1089/omi.2011.0118
37. Sturm G, Szabo T, Fotakis G et al (2020) Scirpy: a Scanpy extension for analyzing single-cell T-cell receptor-sequencing data. Bioinformatics 36:4817–4818. https://doi.org/10.1093/bioinformatics/btaa611
38. Wolf FA, Angerer P, Theis FJ (2018) SCANPY: large-scale single-cell gene expression data analysis. Genome Biol 19:15. https://doi.org/10.1186/s13059-017-1382-0
39. Zhao J, Zhang S, Liu Y et al (2020) Single-cell RNA sequencing reveals the heterogeneity of liver-resident immune cells in human. Cell Discov 6:22. https://doi.org/10.1038/s41421-020-0157-z
40. LaFleur MW, Nguyen TH, Coxe MA et al (2019) PTPN2 regulates the generation of exhausted CD8 T cell subpopulations and restrains tumor immunity. Nat Immunol 20:1335–1347. https://doi.org/10.1038/s41590-019-0480-4
41. Dixon KO, Tabaka M, Schramm MA et al (2021) TIM-3 restrains anti-tumour immunity by regulating inflammasome activation. Nature 595:101–106. https://doi.org/10.1038/s41586-021-03626-9
42. Wauters E, Van Mol P, Garg AD et al (2021) Discriminating mild from critical COVID-19 by innate and adaptive immune single-cell profiling of bronchoalveolar lavages. Cell Res 31:272–290. https://doi.org/10.1038/s41422-020-00455-9
43. Zhang L, Yu X, Zheng L et al (2018) Lineage tracking reveals dynamic relationships of T cells in colorectal cancer. Nature 564:268–272. https://doi.org/10.1038/s41586-018-0694-x
44. Kuijk LM, Verstege MI, Rekers NV et al (2013) Notch controls generation and function of human effector $CD8^+$ T cells. Blood 121:2638–2646. https://doi.org/10.1182/blood-2012-07-442962
45. Duhen T, Duhen R, Montler R et al (2018) Co-expression of CD39 and CD103 identifies tumor-reactive CD8 T cells in human solid tumors. Nat Commun 9:2724. https://doi.org/10.1038/s41467-018-05072-0
46. Hanada KI, Zhao C, Gil-Hoyos R et al (2022) A phenotypic signature that identifies neoantigen-reactive T cells in fresh human lung cancers. Cancer Cell 40:479–93.e6. https://doi.org/10.1016/j.ccell.2022.03.012
47. Oliveira G, Stromhaug K, Klaeger S et al (2021) Phenotype, specificity and avidity of antitumour $CD8^+$ T cells in melanoma. Nature 596:119–125. https://doi.org/10.1038/s41586-021-03704-y
48. Li H, van der Leun AM, Yofe I et al (2019) Dysfunctional CD8 T cells form a proliferative, dynamically regulated compartment within human melanoma. Cell 176:775–89.e18. https://doi.org/10.1016/j.cell.2018.11.043
49. Thommen DS, Koelzer VH, Herzig P et al (2018) A transcriptionally and functionally distinct PD-1^+ $CD8^+$ T cell pool with predictive potential in non-small-cell lung cancer treated with

PD-1 blockade. Nat Med 24:994–1004. https://doi.org/10.1038/s41591-018-0057-z
50. Attrill GH, Owen CN, Ahmed T et al (2022) Higher proportions of CD39+ tumor-resident cytotoxic T cells predict recurrence-free survival in patients with stage III melanoma treated with adjuvant immunotherapy. J Immunother Cancer. https://doi.org/10.1136/jitc-2022-004771
51. Wei J, Montalvo-Ortiz W, Yu L et al (2021) Sequence of αPD-1 relative to local tumor irradiation determines the induction of abscopal antitumor immune responses. Sci Immunol. https://doi.org/10.1126/sciimmunol.abg0117
52. Chua KLM, Fehlings M, Yeo ELL et al (2020) High-dimensional characterization of the systemic immune landscape informs on synergism between radiation therapy and immune checkpoint blockade. Int J Radiat Oncol Biol Phys 108:70–80. https://doi.org/10.1016/j.ijrobp.2020.06.007
53. Seung SK, Curti BD, Crittenden M et al (2012) Phase 1 study of stereotactic body radiotherapy and interleukin-2–tumor and immunological responses. Sci Transl Med. 4:137ra74. https://doi.org/10.1126/scitranslmed.3003649
54. Formenti SC, Rudqvist N-P, Golden E et al (2018) Radiotherapy induces responses of lung cancer to CTLA-4 blockade. Nat Med 24:1845–1851. https://doi.org/10.1038/s41591-018-0232-2
55. Li R, Liu Y, Yin R et al (2021) The dynamic alternation of local and systemic tumor immune microenvironment during concurrent chemoradiotherapy of cervical cancer: a prospective clinical trial. Int J Radiat Oncol Biol Phys 110:1432–1441. https://doi.org/10.1016/j.ijrobp.2021.03.003
56. Kaech SM, Wherry EJ, Ahmed R (2002) Effector and memory T-cell differentiation: implications for vaccine development. Nat Rev Immunol 2:251–262. https://doi.org/10.1038/nri778
57. Kiess AP, Wolchok JD, Barker CA et al (2015) Stereotactic radiosurgery for melanoma brain metastases in patients receiving ipilimumab: safety profile and efficacy of combined treatment. Int J Radiat Oncol Biol Phys 92:368–375. https://doi.org/10.1016/j.ijrobp.2015.01.004
58. Scheper W, Kelderman S, Fanchi LF et al (2019) Low and variable tumor reactivity of the intratumoral TCR repertoire in human cancers. Nat Med 25:89–94. https://doi.org/10.1038/s41591-018-0266-5
59. Rudqvist N-P, Pilones KA, Lhuillier C et al (2018) Radiotherapy and CTLA-4 Blockade Shape the TCR Repertoire of Tumor-Infiltrating T Cells. Cancer Immunol Res 6:139–150. https://doi.org/10.1158/2326-6066.CIR-17-0134
60. Vanpouille-Box C, Pilones KA, Wennerberg E et al (2015) In situ vaccination by radiotherapy to improve responses to anti-CTLA-4 treatment. Vaccine 33:7415–7422. https://doi.org/10.1016/j.vaccine.2015.05.105

Authors and Affiliations

Chao Liu[1] · Yanjuan Chen[2] · Xiaohui Li[3] · Zhijie Bai[4] · Meilin Jiang[5] · Dongsheng Sheng[6] · Wenxue Zou[7] · Rui Huang[7] · Qingyu Huang[7] · Fuhao Wang[7] · Jingyang Zhu[8] · Huiru Sun[8] · Bing Liu[4] · Zongcheng Li[4] · Bing Sun[8]

✉ Bing Liu
bingliu17@yahoo.com

✉ Zongcheng Li
lizc07@vip.qq.com

✉ Bing Sun
sunice116@163.com

Chao Liu
charles_liu@hsc.pku.edu.cn

Yanjuan Chen
chenyj_613@qq.com

Xiaohui Li
lixiaohui2020@163.com

Zhijie Bai
baizhijie@sina.cn

Meilin Jiang
1906131843@qq.com

Dongsheng Sheng
shengdongsheng1978@163.com

Wenxue Zou
wenxuezou@163.com

Rui Huang
huangrui1620@outlook.com

Qingyu Huang
qingyu_huang@outlook.com

Fuhao Wang
940000311@qq.com

Jingyang Zhu
32410946@qq.com

Huiru Sun
sunhui19851106@sina.com

[1] Department of Radiation Oncology, Peking University First Hospital, Beijing 100034, China

[2] Department of Geriatrics and Division of Rheumatology and Research, The Second Clinical Medical College, Jinan University (Shenzhen People's Hospital), Shenzhen 518020, China

[3] Department of Medical Oncology, Peking University First Hospital, Beijing 100034, China

[4] State Key Laboratory of Experimental Hematology, Institute of Hematology, Fifth Medical Center of Chinese PLA General Hospital, Beijing 100071, China

[5] Key Laboratory for Regenerative Medicine of Ministry of Education, Institute of Hematology, School of Medicine, Jinan University, Guangzhou 510632, Guangdong, China

[6] Department of Thoracic Surgery, Fifth Medical Center of Chinese PLA General Hospital, Beijing 100071, China

[7] Department of Radiation Oncology, Shandong Cancer Hospital and Institute, Shandong First Medical University

and Shandong Academy of Medical Sciences, Jinan 250117, China

[8] Department of Radiation Oncology, Fifth Medical Center of Chinese PLA General Hospital, Beijing 100071, China